

**Electronic Supplemetary Information for
Structural characterization and magnetic properties of chromium jarosite $KCr_3(OD)_6(SO_4)_2$**

Sofie Janas^{ab}, Mathilde B. Sørensen^a, Anders B. A. Andersen^c, Mikkel Juelskolt^f, Martin Boehm^d, Kasper S. Pedersen^e, Kirsten M. Ø. Jensen^f, Kim Lefmann^a, Ulla Gro Nielsen^c

^a Niels Bohr Institute, University of Copenhagen, DK-2100 Copenhagen Ø, Denmark.

^b Laboratory for Quantum Magnetism, Institute of Physics, EPFL, 1015 Lausanne, Switzerland.

^c Institute of Physics, Chemistry, and Pharmacy, University of Southern Denmark, Campusvej 55, 5230 Odense M, Denmark.
E-mail: ugn@sdu.dk

^d Institut Max von Laue Paul Langevin, 38042 Grenoble, France.

^e Institute of Chemistry, Technical University of Denmark, DK-2800 Kgs. Lyngby, Denmark.

^f Department of Chemistry and Nano-Science Center, University of Copenhagen, DK-2100 Copenhagen Ø, Denmark.

Contents

ESI-A Synthesis details	2
ESI-B Rietveld refinement of PXRD data for remaining samples	2
ESI-C Rietveld refinement of powder neutron diffraction	5
ESI-D Additional ² H MAS NMR data	6
ESI-E Scanning Electron microscopy of selected samples	8
ESI-F Temperature-dependent neutron diffraction	10

ESI-A Synthesis details

Synthesis details of all samples are shown in table ESI-1. ESI-A.

Table ESI-1: Synthesis detail for all prepared samples. All syntheses were carried out in 40 mL hydrothermal reaction vessels, see synthesis section in main article for further details.

Batch 1		B1-1	B1-2	B1-3
Sample				
Yield		0.168 g	0.239 g	0.022 g
Percent theoretical yield		34.1%	48.5%	4.5%
Temperature		200 °C	200 °C	200 °C
Synthesis time		165.5 h	94 h	24 h
Batch 2		B2-1	B2-2	B2-3
Sample				
Yield		0.2403 g	0.2839 g	0.1954 g
Percent theoretical yield		48.7%	57.6%	40.0%
Temperature		190 °C	190 °C	190 °C
Synthesis time		164 h	95 h	65 h
Batch 3		B3-1	B3-2	B3-3
Sample				
Yield		0.3716 g	0.2536 g	0.2100 g
Percent theoretical yield		75.3%	51.4%	42.6 %
Temperature		210 °C	210 °C	210 °C
Synthesis time		164.5 h	95 h	65.5 h

ESI-B Rietveld refinement of PXRD data for remaining samples

The Rietveld refinement of PXRD data was performed using the Fullprof suite.¹ Data is shown in figure ESI-1 and parameters in tables ESI-2 to ESI-9. The background was described using a 7th degree Chebyshev polynomial. The peak shape was modelled using the Thompson-Cox-Hasting pseudo-Voigt function. In all cases the peak shape could be described by only refining the U and Y parameter. The experimental contributions to the peak shape was obtained from an Aluminium standard; also modelled using the Thompson-Cox-Hasting pseudo-Voigt function. In addition to the structural parameters, background and peak shape, a zero error was also refined for each sample. Sample B2-2 contained a small amount of impurity which was visible as a small peak at 1.63 Å.

Table ESI-2: Refined parameters for the Rietveld refinement of PXRD from sample B1-1

B1-1					
a 7.2215 Å	b 7.2215 Å	c 17.2124 Å	zero error 0.0215	R _{Bragg} 11.3%	
U 0.0329	V 0	W 0	X 0	Y 0.0259	
Atom	x	y	z	Debye-Waller factor	occ
K	0	0	0	1 Å ²	1
S	0	0	0.31	1 Å ²	1
Cr	0.5	0	0.5	0.7612 Å ²	1
O1	0	0	0.396	1 Å ²	1
O2	0.2249	0.7751	-0.0599	1 Å ²	1
O3	0.13556	0.8644	0.1313	1 Å ²	1
D	0.185	0.815	0.111	2 Å ²	1

Table ESI-3: Refined parameters for the Rietveld refinement of PXRD from sample B1-2

B1-2					
a 7.2187 Å	b 7.2187 Å	c 17.2341 Å	zero error -0.0356	R _{Bragg} 11.2%	
U 0.0106	V 0	W 0	X 0	Y 0.0096	
Atom	x	y	z	Debye-Waller factor	occ
K	0	0	0	1 Å ²	1
S	0	0	0	0.30511	1 Å ²
Cr	0.5	0	0	0.1052 Å ²	1
O1	0	0	0.3866	1 Å ²	1
O2	0.2202	0.7798	-0.0564	1 Å ²	1
O3	0.1333	0.8668	0.1338	1 Å ²	1
D	0.185	0.815	0.111	2 Å ²	1

Table ESI-4: Refined parameters for the Rietveld refinement of PXRD from sample B2-1

B2-1					
a 7.2191Å	b 7.2191Å	c 17.1886Å	zero error 0.0862	R _{Bragg} 6.99%	
U 0.0185	V 0	W 0	IG 0	X 0	Y 0.0050
Atom	x 0.185	y 0.815	z 0.111	Debye-Waller factor 2 Å ²	occ 1
K	0	0	0	2.0589 Å ²	1
S	0	0	0.30721	1.3184 Å ²	1
Cr	0.5	0	0.5	3.1026 Å ²	1
O1	0	0	0.3881	2.2626 Å ²	1
O2	0.2229	0.7771	-0.0573	2.2626 Å ²	1
O3	0.1276	0.8723	0.1341	2.2626 Å ²	1
D	0.185	0.815	0.111	2 Å ²	1

Table ESI-5: Refined parameters for the Rietveld refinement of PXRD from sample B2-2

B2-2					
a 7.2199Å	b 7.2199Å	c 17.2205Å	zero error 0.0424	R _{Bragg} 7.11%	
U 0.0196	V 0	W 0	IG 0	X 0	Y 0.0124
Atom	x 0.196	y 0.816	z 0.111	Debye-Waller factor 2 Å ²	occ 1
K	0	0	0	0.8049 Å ²	1
S	0	0	0.3096	1.6906 Å ²	1
Cr	0.5	0	0.5	2.8001 Å ²	1
O1	0	0	0.3936	1.6419 Å ²	1
O2	0.2220	0.7781	-0.0555	1.6419 Å ²	1
O3	0.1275	0.8725	0.1336	1.6419 Å ²	1
D	0.185	0.815	0.111	2 Å ²	1

Table ESI-6: Refined parameters for the Rietveld refinement of PXRD from sample B2-3

B2-3					
a 7.2213Å	b 7.2213Å	c 17.1866Å	zero error -0.0110	R _{Bragg} 5.36%	
U 0.0185	V 0	W 0	IG 0	X 0	Y 0.0056
Atom	x 0.185	y 0.815	z 0.111	Debye-Waller factor 2 Å ²	occ 1
K	0	0	0	2.1785 Å ²	1
S	0	0	0.3060	0.2224 Å ²	1
Cr	0.5	0	0.5	1.6000 Å ²	1
O1	0	0	0.3911	0.6467 Å ²	1
O2	0.2254	0.7746	-0.0554	0.6467 Å ²	1
O3	0.1283	0.8717	0.1355	0.6467 Å ²	1
D	0.185	0.815	0.111	2 Å ²	1

Table ESI-7: Refined parameters for the Rietveld refinement of PXRD from sample B3-1

B3-1					
a 7.2215Å	b 7.2215Å	c 17.2343Å	zero error 0.0166	R _{Bragg} 7.80%	
U 0.0203	V 0	W 0	IG 0	X 0	Y 0.0114
Atom	x 0.203	y 0.816	z 0.111	Debye-Waller factor 2 Å ²	occ 1
K	0	0	0	0.3105 Å ²	1
S	0	0	0.3092	1.7000 Å ²	1
Cr	0.5	0	0.5	2.8618 Å ²	1
O1	0	0	0.3877	1.0768 Å ²	1
O2	0.2232	0.7768	-0.0583	1.0768 Å ²	1
O3	0.1299	0.8700	0.1328	1.0768 Å ²	1
D	0.185	0.815	0.111	2 Å ²	1

Table ESI-8: Refined parameters for the Rietveld refinement of PXRD from sample B3-2

B3-2					
a 7.2214Å	b 7.2214Å	c 17.1822Å	zero error 0.0768	R _{Bragg} 5.54%	
U 0.0171	V 0	W 0	IG 0	X 0	Y 0.0086
Atom	x 0.171	y 0.815	z 0.111	Debye-Waller factor 2 Å ²	occ 1
K	0	0	0	3.8777 Å ²	1
S	0	0	0.3092	1.2945 Å ²	1
Cr	0.5	0	0.5	3.2895 Å ²	1
O1	0	0	0.3901	1.9168 Å ²	1
O2	0.2266	0.7734	-0.0557	1.9168 Å ²	1
O3	0.1293	0.8707	0.1341	1.9168 Å ²	1
D	0.185	0.815	0.111	2 Å ²	1

Table ESI-9: Refined parameters for the Rietveld refinement of PXRD from sample B3-3

B3-3					
a 7.2222Å	b 7.2222Å	c 17.2119Å	zero error 0.0665	R _{Bragg} 5.88%	
U 0.0364	V 0	W 0	IG 0	X 0	Y 0.0102
Atom	x 0.364	y 0.816	z 0.111	Debye-Waller factor 2 Å ²	occ 1
K	0	0	0	3.4670 Å ²	1
S	0	0	0.3077	2.8906 Å ²	1
Cr	0.5	0	0.5	4.8290 Å ²	1
O1	0	0	0.3861	3.1119 Å ²	1
O2	0.2251	0.7749	-0.0574	3.1119 Å ²	1
O3	0.1272	0.8727	0.1331	3.1119 Å ²	1
D	0.185	0.815	0.111	2 Å ²	1

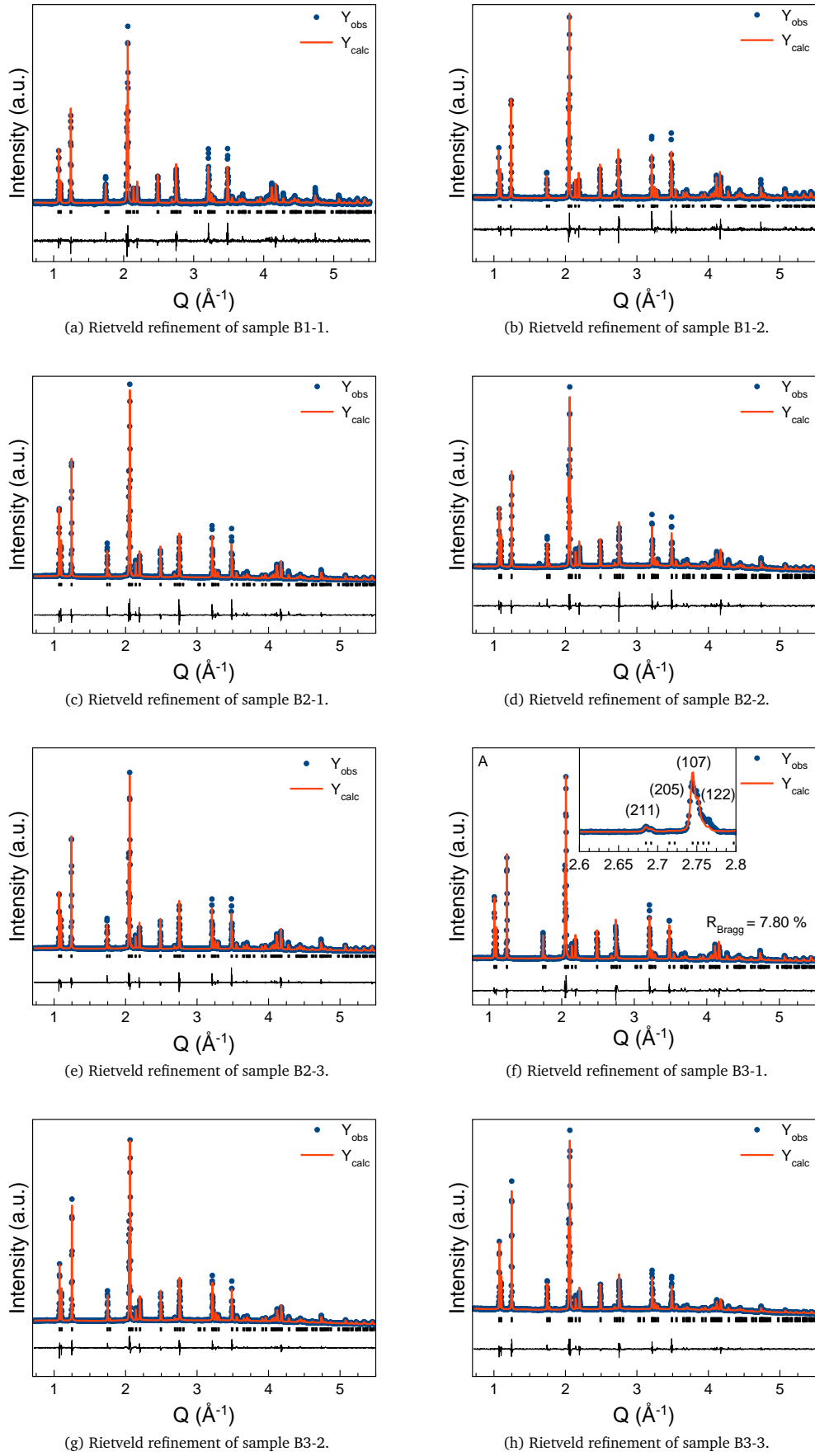


Figure ESI-1: Rietveld refinements of all Cr-jarosite samples.

ESI-C Rietveld refinement of powder neutron diffraction

The temperature-dependent neutron powder diffraction experiment was carried out on a powder sample with mass 234.7 mg using two wavelengths, $\lambda = 1.36 \text{ \AA}$ and $\lambda = 1.87 \text{ \AA}$. The Rietveld refinement was performed using Topas academic to refine both datasets simultaneously. Each dataset had the background described using a 7th degree Chebyshev polynomial. The peak shape was modelled using the Thompson-Cox-Hastings pseudo-Voigt function. The structural parameters were constrained to be the same for each dataset. In addition to the structural parameters, background and peak shape, a zero error was also refined for each dataset. The D_3O^+ replacing the K^+ is modelled only as an O at the K-site because at room temperature the deuterium atoms are rotating around the (0, 0, 0) position.^{2,3} The lack of fixed positions in the unit cell makes all the scattering from the deuterium atoms diffuse and non-contributing with regards to the Bragg intensity. The Al sample holder was refined using a Le Bail refinement using a cubic Al phase with $a = 4.0632 \text{ \AA}$.

Table ESI-10: Refined parameters for the Rietveld refinement of PND from sample B3-1 with $\lambda = 1.36 \text{ \AA}$

$\lambda = 1.36 \text{ \AA}$					
a	b	c	zero error	R_{Bragg}	
7.2427 \AA	7.2427 \AA	17.2835 \AA	0.3756	2.39%	
U	V	W			
-0.3528	0.1285	-0.4545			
Z	Y	X			
0.2843	0	0.0981			
Atom	x	y	z	Debye-Waller factor	occ
K	0	0	0	1.6980 \AA^2	0.89
O4	0	0	0	1.6980 \AA^2	0.21
S	0	0	0.3055	0.6003 \AA^2	1
Cr	0.5	0	0.5	1.4949 \AA^2	1
O1	0	0	0.3902	1.2426 \AA^2	1
O2	0.224	0.776	-0.0574	1.2426 \AA^2	1
O3	0.1272	0.8727	0.1370	See table ESI-12	1
D	0.1952	0.8048	0.1107	See table ESI-12	

Table ESI-11: Refined parameters for the Rietveld refinement of PND from sample B3-1 with $\lambda = 1.87 \text{ \AA}$

$\lambda = 1.87 \text{ \AA}$					
a	b	c	zero error	R_{Bragg}	
7.2427 \AA	7.2427 \AA	17.2835 \AA	0.4042	2.43%	
U	V	W			
-0.63055	0.1198	-0.8157			
Z	Y	X			
0.5318	0	0.00075			
Atom	x	y	z	Debye-Waller factor	occ
K	0	0	0	1.6980 \AA^2	0.89
O4	0	0	0	1.6980 \AA^2	0.21
S	0	0	0.3055	0.6003 \AA^2	1
Cr	0.5	0	0.5	1.4949 \AA^2	1
O1	0	0	0.3902	1.2426 \AA^2	1
O2	0.224	0.776	-0.0574	1.2426 \AA^2	1
O3	0.1272	0.8727	0.1370	See table ESI-12	1
D	0.1952	0.8048	0.1107	See table ESI-12	

Table ESI-12: Anisotropic Debye-Waller factor for the Rietveld refinement of PND from sample B3-1 with $\lambda = 1.36 \text{ \AA}$ and $\lambda = 1.87 \text{ \AA}$

Anisotropic DW factor	O3	D
B_{11}	0.6238 \AA^2	1.6439 \AA^2
B_{22}	0.6238 \AA^2	1.6439 \AA^2
B_{33}	1.3691 \AA^2	2.8471 \AA^2
B_{12}	0.4595 \AA^2	0.5527 \AA^2
B_{13}	0.0355 \AA^2	0.0608 \AA^2
B_{23}	-0.0355 \AA^2	-0.0608 \AA^2

ESI-D Additional ^2H MAS NMR data

Variable temperature ^2H MAS NMR spectra were recorded in the temperature setting from -40 to 100 °C using a 3.2 mm HXY MAS NMR probe using 16 and 17 kHz spinning speeds. The exact sample temperature was determined using the $\delta_{iso}(^{207}\text{Pb})$ of lead(II) nitrate as a NMR thermometer.⁴ The temperature dependence of the Cr₂-OD (K) site was found to -2.34 ppm/K by linear fit of $\delta(^2\text{H})$ as a function of temperature (Fig. ESI-4).

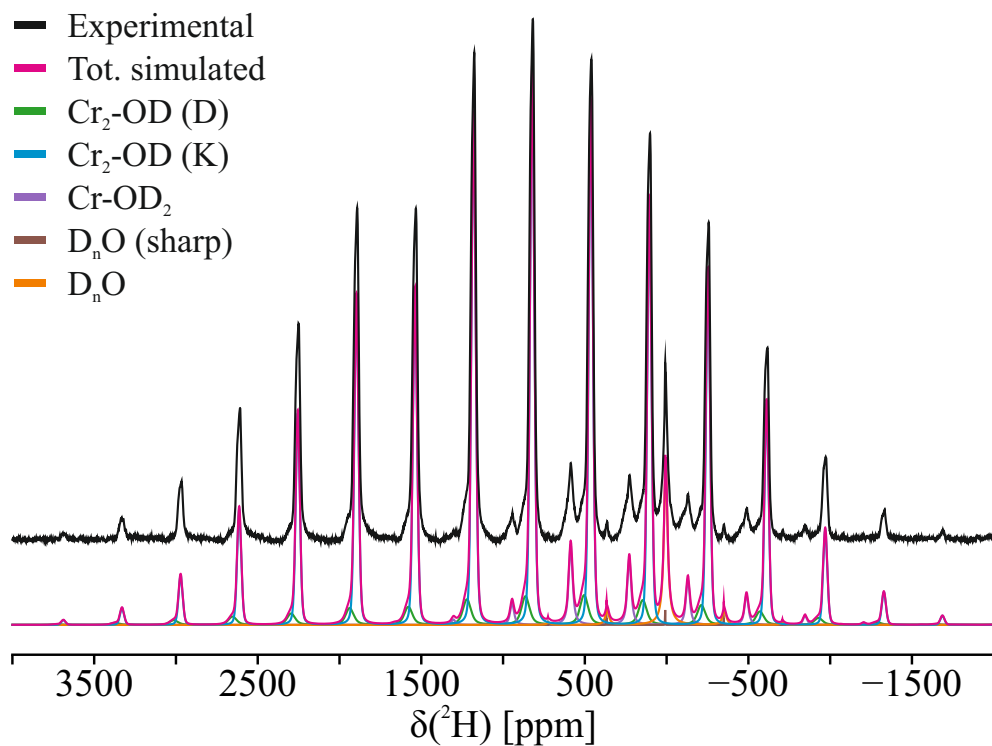


Figure ESI-2: Experimental and simulated ^2H MAS NMR spectrum of sample B3-1 recorded with 33 KHz spinning speed using the parameters in Table ESI-13.

Table ESI-13: ^2H NMR parameters obtained from fitting of the experimental spectra for the individual spectra. The total shift anisotropy is given in the Haeberlen convention c.f., main text, where β is an angle between the principal axes of the CSA and quadrupole tensor. The other two Euler angles, α (γ) are undefined for η_σ (η_Q) = 0 and could not be unambiguously determined. The error on the average values is estimated from the standard deviation. The relative concentration of the different sites for all samples is illustrated in Fig. ESI-3. The line shape of the Cr₂-OD (K) resonance is clearly asymmetric, reflecting a distribution of $\delta_{iso}(^2\text{H})$ due to different local environments, but the other NMR parameters are similar. For B2-1 this is clearly seen as a resonance at $\delta_{iso}(^2\text{H})$ = 804 ppm, which constitute ca. 40 % of the total intensity.

Sample	Group	$\delta_{iso}(^2\text{H})$ [ppm]	Δ [ppm]	η_σ	C_Q [MHz]	η_Q	β [deg]	Intensity [%]
B1-1	Cr ₂ -OD (D)	876(10)	-900(100)	1.00(10)	0.240(40)	0.10(10)	39(5)	9(1)
	Cr ₂ -OD (K)	828(3)	-960(50)	1.00(10)	0.222(10)	0.10(10)	52(5)	76(1)
	Cr-OD ₂	230(3)	600(50)	0.00(10)	0.109(5)	0.63(10)	64(5)	7(1)
	D _n O (sharp)	9(1)	0(10)	0.00(10)	0.100(5)	0.00(10)	0(5)	1>
	D _n O	7(2)	0(10)	0.00(10)	0.050(5)	0.00(10)	0(5)	8(1)
B1-2	Cr ₂ -OD (D)	876(10)	-1090(100)	1.00(10)	0.240(40)	0.10(10)	39(5)	13(1)
	Cr ₂ -OD (K)	828(3)	-960(50)	1.00(10)	0.222(10)	0.10(10)	52(5)	77(1)
	Cr-OD ₂	230(3)	780(50)	0.00(10)	0.092(5)	0.80(10)	70(5)	9(1)
	D _n O (sharp)	9(1)	0(10)	0.00(10)	0.100(5)	0.00(10)	0(5)	1>
	D _n O	7(2)	0(10)	0.00(10)	0.050(5)	0.00(10)	0(5)	1(1)
B2-1	Cr ₂ -OD (D)	864(10)	-1120(100)	1.00(10)	0.240(40)	0.10(10)	48(5)	15(1)
	Cr ₂ -OD (K)	823(3)	-930(50)	1.00(10)	0.223(10)	0.11(10)	53(5)	73(2)
	Cr-OD ₂	226(3)	670(50)	0.00(10)	0.107(5)	1.00(10)	59(5)	8(1)
	D _n O (sharp)	8(1)	0(10)	0.00(10)	0.100(5)	0.00(10)	0(5)	1>
	D _n O	6(2)	0(10)	0.00(10)	0.050(5)	0.00(10)	0(5)	4(1)
B2-2	Cr ₂ -OD (D)	860(10)	-1070(100)	1.00(10)	0.240(40)	0.10(10)	47(5)	18(1)
	Cr ₂ -OD (K)	822(5)	-940(50)	1.00(10)	0.219(15)	0.10(10)	54(5)	64(2)
	Cr ₂ -OD (???)	804(5)	-1000(50)	1.00(10)	0.226(15)	0.10(10)	49(5)	-
	Cr-OD ₂	226(3)	510(50)	0.00(10)	0.110(5)	1.00(10)	70(5)	11(1)
	D _n O (sharp)	9(1)	0(10)	0.00(10)	0.100(5)	0.00(10)	0(5)	1>
	D _n O	6(2)	0(10)	0.00(10)	0.050(5)	0.00(10)	0(5)	7(1)
B2-3	Cr ₂ -OD (D)	865(10)	-900(100)	1.00(10)	0.240(40)	0.10(10)	38(5)	19(1)
	Cr ₂ -OD (K)	823(3)	-930(50)	1.00(10)	0.222(10)	0.09(10)	53(5)	63(2)
	Cr-OD ₂	228(3)	690(50)	0.00(10)	0.100(5)	0.60(10)	65(5)	11(1)
	D _n O (sharp)	9(1)	0(10)	0.00(10)	0.100(5)	0.00(10)	0(5)	1>
	D _n O	5(2)	0(10)	0.00(10)	0.050(5)	0.00(10)	0(5)	7(1)
B3-1	Cr ₂ -OD (D)	862(10)	-1100(100)	1.00(10)	0.240(40)	0.10(10)	46(5)	10(1)
	Cr ₂ -OD (K)	821(3)	-1000(50)	1.00(10)	0.222(10)	0.14(10)	53(5)	79(2)
	Cr-OD ₂	228(3)	720(50)	0.00(10)	0.100(5)	0.69(10)	68(5)	6(1)
	D _n O (sharp)	9(1)	0(10)	0.00(10)	0.100(5)	0.00(10)	0(5)	1>
	D _n O	5(2)	0(10)	0.00(10)	0.050(5)	0.00(10)	0(5)	5(2)
B3-2	Cr ₂ -OD (D)	870(10)	-1110(100)	1.00(10)	0.230(40)	0.10(10)	40(5)	19(1)
	Cr ₂ -OD (D)	827(3)	-850(50)	1.00(10)	0.224(10)	0.07(10)	55(5)	63(1)
	Cr-OD ₂	230(3)	700(50)	0.00(10)	0.105(5)	1.00(10)	55(5)	11(1)
	D _n O (sharp)	10(1)	0(10)	0.00(10)	0.100(5)	0.00(10)	0(5)	1>
	D _n O	8(2)	0(10)	0.00(10)	0.050(5)	0.00(10)	0(5)	7(1)
Average values	Cr ₂ -OD (D)	868(7)	-1040(100)	1.00(10)	0.240(3)	0.10(10)	42(4)	-
	Cr ₂ -OD (K)	825(3)	-940(50)	1.00(10)	0.222(2)	0.10(4)	53(1)	-
	Cr ₂ -OD (???)	804(5)	-1000(50)	1.00(10)	0.226(5)	0.10(10)	49(6)	-
	Cr-OD ₂	228(2)	670(90)	0.00(30)	0.103(7)	0.82(18)	64(6)	-
	D _n O (sharp)	9(1)	0(10)	0.00(10)	0.100(5)	0.00(10)	0(5)	-
	D _n O	6(2)	0(10)	0.00(10)	0.050(5)	0.00(10)	0(5)	-

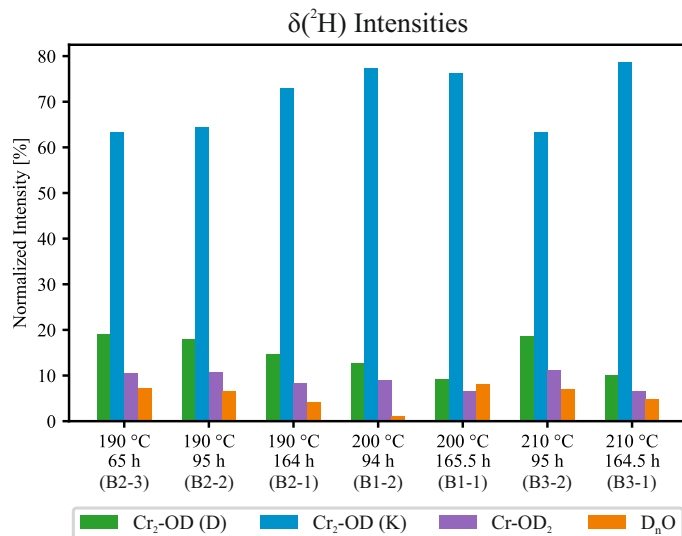


Figure ESI-3: The relative intensity of the different local ^2H environments in the samples using the data in Table ESI-13.

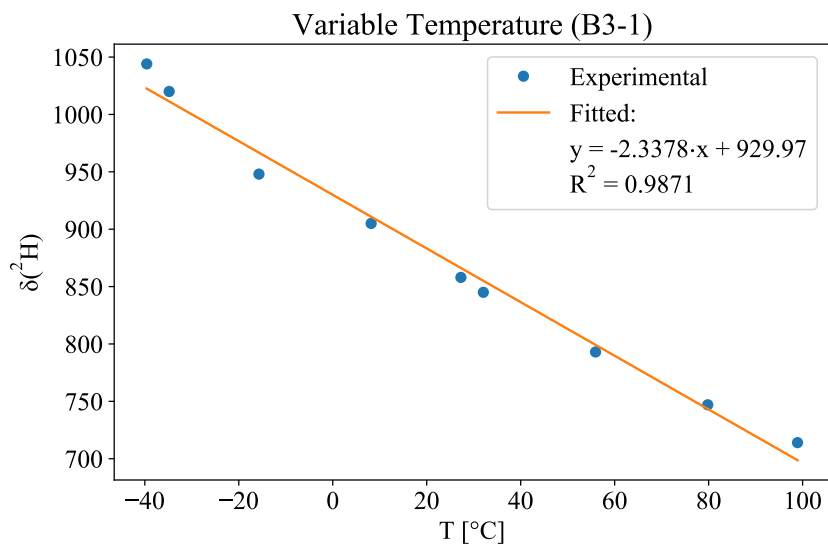


Figure ESI-4: $\delta_{\text{iso}}(^2\text{H})$ for the $\text{Cr}_2\text{-OD (K)}$ site as a function of temperature illustrating the linear temperature dependence of $\delta(^2\text{H})$.

ESI-E Scanning Electron microscopy of selected samples

SEM was performed on samples B3-1 and B2-1, see figure ESI-5.

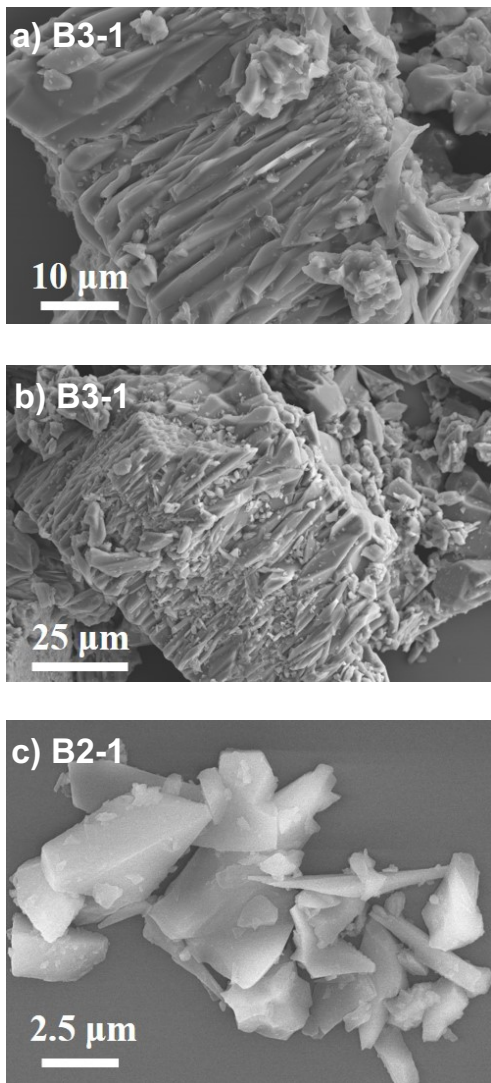


Figure ESI-5: (a) and (b) SEM images of Sample B3-1, which show that the large particles are agglomerates of several, smaller particles in agreement with the pronounced stacking disorder observed in PXRD and neutron diffraction as well as the distribution on $\delta_{iso}(^2\text{H})$. (c) SEM image of individual, smaller crystals from sample B2-1. Notice that different magnification was used in the three images, as indicated by the scale bar.

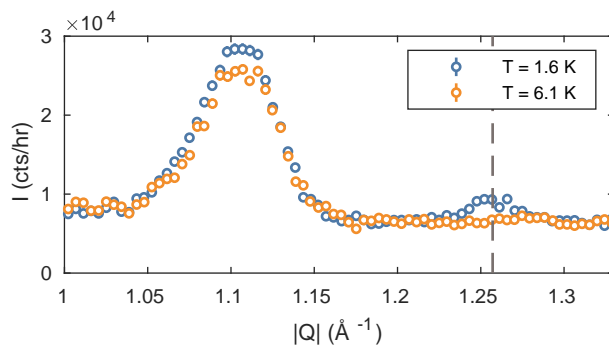


Figure ESI-6: 2θ scan across the elastic Bragg peaks at two temperatures above and below the phase transition, showing the growth of the (012) Bragg peak. Grey dashed line indicates the peak position. Errorbars are smaller than markers.

ESI-F Temperature-dependent neutron diffraction

The temperature-dependent neutron powder diffraction experiment was carried out on a powder sample with mass 234.7 mg. First $|Q|$ was scanned across the peak position of the magnetic (012) peak at two temperatures above and below T_N in order to determine the exact peak position. This is shown in figure ESI-6, where the (012) peak position, $|Q| \approx 1.257 \text{ \AA}^{-1}$, is indicated by the grey dashed line. The strong peak at $|Q| \approx 1.1 \text{ \AA}^{-1}$ is the sum of the structural (003) and (101) peaks, on top of which the magnetic (101) and ($\bar{1}\bar{1}\bar{1}$) peaks develops. The temperature-dependent signal of (012) is then obtained by counting at the peak position for a given temperature after stabilization. Temperature stabilization was carefully checked, and only data points with temperature fluctuations less than 0.2 K are included in the fit in in the main article.

Notes and references

- [1] J. Rodríguez-Carvajal, *Physica B*, 1993, **192**, 55 – 69.
- [2] U. G. Nielsen, I. Heinmaa, A. Samoson, J. Majzlan and C. P. Grey, *Chemistry of Materials*, 2011, **23**, 3176–3187.
- [3] J. D. Gale, K. Wright and K. A. Hudson-Edwards, *American Mineralogist*, 2010, **95**, 1109–1112.
- [4] A. Bielecki and D. P. Burum, *Journal of Magnetic Resonance, Series A*, 1995, **116**, 215–220.